Dimension reduction for extracting geometrical structure of multidimensional phase space: Application to fast energy exchange in the reaction $O(^1D)+N_2O \rightarrow NO+NO$

Shinnosuke Kawai,* Yo Fujimura,† and Okitsugu Kajimoto
Department of Chemistry, Graduate School of Science, Kyoto University, Kitashirakawa-Oiwakecho, Sakyo-ku, Kyoto 606-8502, Japan

Takefumi Yamashita
Department of Basic Science, Graduate School of Arts and Sciences, University of Tokyo, Komaba, Tokyo 153-8902, Japan

Chun-Biu Li
Nonlinear Science Laboratory, Department of Earth and Planetary Sciences, Faculty of Science, Kobe University, Nada, Kobe 657-8501, Japan

Tamiki Komatsuzaki
Nonlinear Science Laboratory, Department of Earth and Planetary Sciences, Faculty of Science, Kobe University, Nada, Kobe 657-8501, Japan
and Department of Theoretical Studies, Institute for Molecular Science, Myodaiji, Okazaki 444-8585, Japan

Mikito Toda
Department of Physics, Faculty of Science, Nara Women's University, Nara 630-8506, Japan
(Received 26 October 2006; revised manuscript received 15 December 2006; published 16 February 2007)

One of the most fundamental problems in studying general Hamiltonian systems with many degrees of freedom is to extract a low-dimensional subsystem including the essential dynamics. In this paper, a new partial normal form (PNF) method is developed to reduce the number of coupling terms in the Hamiltonian and to simplify the dynamics analyses. The PNF method allows one to decouple many unimportant bath modes as well as the reactive mode from the system by assessing the significance of the coupling terms. The method is applied to the chemical reaction $O(^1D)+N_2O \rightarrow NO+NO$, which was found to exhibit efficient energy exchange between the two NO stretching modes despite the short lifetime of the reaction intermediate [S. Kawai *et al.*, J. Chem. Phys. **124**, 184315 (2006)]. Through the analysis of the two-dimensional PNF Hamiltonian subsystem, it is found that the motion of the subsystem preserves the "normal mode picture" of the symmetric and antisymmetric NO stretching modes despite its high energy. Then the vibrational energy, initially localized in the newly formed NO bond, is transferred to the reactants' NO bond through the beating between the symmetric and antisymmetric stretching modes. The preservation of the normal mode picture and the short period of the beating explain the fast energy exchange between the two NO bonds. This successful application proves that the PNF method can extract the essential small subspace from many-degrees-of-freedom Hamiltonian systems.

DOI: 10.1103/PhysRevA.75.022714 PACS number(s): 34.10.+x

I. INTRODUCTION

The investigation of geometrical structure of multidimensional phase space provides crucial information to solve various problems in general physics ranging from chemical reactions to planet motions. For a system with two degrees-of-freedom (DOF), it is well known that its phase-space structure can easily be visualized by the Poincaré surface of section (SOS). However, it becomes difficult to capture the essence of dynamics in higher-dimensional systems because the increase of the SOS dimension makes the visualizations of the SOS impossible. Hence it would be desirable to introduce a low-dimensional model, which may effectively describe the essential dynamics of the systems in question. For the problems of characterizing molecular vibrations around an equilibrium point, two-DOF models with some of the bond lengths and/or angles fixed in advance have been often used to study the phase-space structure below the dissociation energy [1–10]. It has been shown that the simple description by normal modes becomes invalid as the energy increases, and that new types of periodic orbits (POs) emerge through bifurcation then. The new types of POs have been characterized as local modes [1–4], precessional modes [6], dissociation modes [8,9], and so forth, according to the energy and the types of couplings. Such effective two-DOF models have been constructed based on empirical intuitions. In contrast to vibrations of bound molecules, dimensions of reacting systems involving bond forming and breaking cannot be reduced by those intuitions. Since they cannot always

*Present address: Laboratoire de Chimie Théorique, Faculté des Sciences, Université de Sherbrooke, Sherbrooke, Québec, Canada J1K 2R1; Electronic address: s.kawai@usherbrooke.ca

†Present address: The Center for Basic Education and Integrated Learning, Kanagawa Institute of Technology, 1030 Shimo-Ogino, Atsugi, Kanagawa 243-0292, Japan; Electronic address: fujimura@gen.kanagawa-it.ac.jp

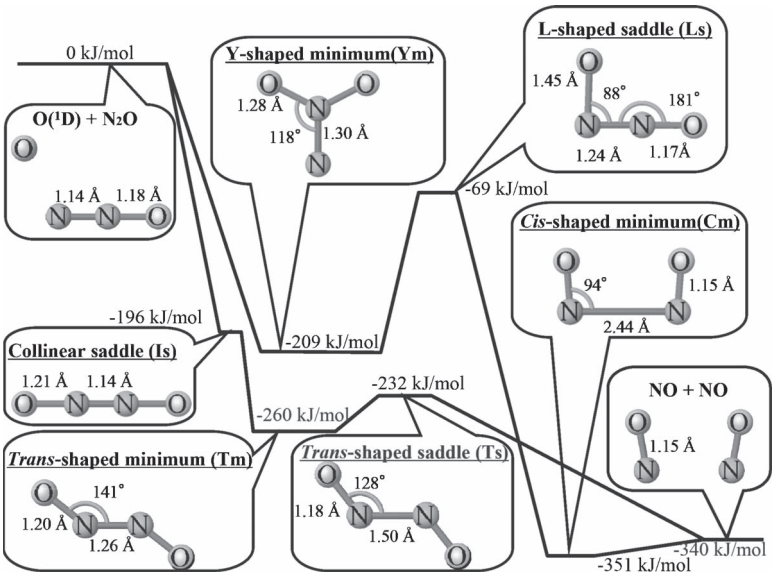

FIG. 1. A schematic representation of the stationary points and the energy profile of the PES of the reaction $O(^1D)+N_2O \rightarrow NO+NO$.

reduce the dimensionality of the system in question through the entire region of the space to a certain lower dimension, an appropriate theory without any empirical intuitions is needed to extract a small essential subspace from the multiple-DOF phase space.

In this respect, the normal form (NF) theory, a classical analog of Van Vleck perturbation theory [11,12], is a powerful tool for such dimension reduction. This theory provides considerable information on phase-space geometry around stationary points by simplifying the form of Hamiltonian as much as possible. It has been applied to many systems to characterize the dynamics around rank-1 saddles as phase-space structures [13–25]. At a rank-1 saddle point, that is, an equilibrium point with one negative Hessian eigenvalue, one reactive mode and the other nonreactive bath modes have one imaginary and multiple real frequencies, respectively. It was found [13–22] that up to a certain high energy, the reactive mode defined in the phase space could be separated from all the bath DOF by the application of the NF theory, even when the nonlinear couplings wash out all the constants of motion in the bath space. In other words, the reactive and bath spaces can be investigated independently if the NF theory is utilized. The dynamics in the bath space in the vicinity of a saddle can be mathematically referred to the motion in the normally hyperbolic invariant manifold (NHIM) [26,27], which generalizes the PO dividing surface in two-DOF systems. Recently, Li *et al.* [24,25] applied this method to a three-DOF model Hamiltonian regarded as a prototype of isomerization reaction. The dynamics in NHIM was easily examined by SOS because the system is reduced to two-DOF after the separation of the reactive mode. However, for systems with more DOF than three, we can no longer carry out the SOS analysis to investigate the dynamics in NHIM, because the NHIM has still more than three DOF.

In this paper, we present a dimension reduction scheme to look into the phase-space geometry of the internal structure of high-dimensional NHIM. In addition to the separation of the reactive mode, we eliminate as many couplings as possible among the bath modes. By simplifying the bath mode couplings, we can construct a subsystem that describes the essential aspects of the process. As an illustrative example, we apply our dimension reduction method to the most characteristic path (named Path 1 in Ref. [28]) of the planar reaction of $O(^1D)$ with N_2O,

$$O(^1D) + NN'O' \rightarrow NO + N'O', \tag{1.1}$$

where prime symbols are used to distinguish the two NO products. Due to the high dimensionality of this system, it is crucial to look further into the possibility of reducing the dimensionality of the bath space after it is separated from the reactive DOF, in order to reveal the complexity of the reaction dynamics. The profile of the analytic potential energy surface (PES) function constructed with CASPT2 calculations [28] is schematically shown in Fig. 1.

The quasiclassical trajectory study of this system revealed that the reactive trajectories of this system can be classified into four categories, which were named paths 1–4. Along path 1, the trajectories pass through three stationary points, the collinear saddle (denoted by the symbol *Is*), the *trans* minimum (*Tm*), and the *trans* saddle (*Ts*). The initial stage of this reaction, where the nearly collinear approach of the $O(^1D)$ atom to N_2O takes place, can be regarded as a motion along a bath mode direction of *Is*. The system then falls into *Tm* following the reactive direction of *Is*. Since the large energy difference between *Is* and the reactant is mostly released along the bath direction, the bath mode oscillation at *Is* is expected to have a large amplitude. Therefore the bath modes are subject to large nonlinear couplings. It is not at all trivial to estimate to what extent we can reduce the dimensionality of the system. For this reason, this system is a suitable example to show how our method works for analyzing NHIM in high-dimensional systems.

The analyses of the motion around *Is* are also interesting from the viewpoint of product energy disposal, which provides important information for clarifying the chemical reaction dynamics. Traditionally it has been believed that the deeper the potential well of the reaction intermediate becomes, the more statistically the product states distribute, since the long residence time in the well allows the consid-

erable energy mixing [29]. However, path 1 of the reaction (1.1) shows nearly equal excitation of two NO vibrations despite its short residence time [28]. Of the two NO products, the one originating in $O(^1D)$ is called "new NO" and the other from the reactant N_2O is called "old NO." At the initial stage of the reaction, the new NO part has an infinite nuclear distance whereas the old NO has almost the same distance as in the product. Thus, the equal vibrational energy of the products indicates that an efficient energy transfer has taken place from the new NO to the old despite the short residence time. This is in clear contrast to the traditional picture [29] mentioned above. As will be shown in Sec. III, the characteristic energy exchange along path 1 occurs when the trajectory is passing by the collinear saddle point (*Is*). Thus, careful analysis of the phase space around *Is* is quite crucial for understanding the underlying mechanism of the efficient energy exchange.

This paper is organized as follows. Our new dimension reduction method is presented in terms of partial NF theory in Sec. II. The model and calculation are described in Sec. III. In Sec. IV, we analyze the dynamics of this system and propose a simple model to explain the fast energy exchange between two NO vibrations. We give a summary and outlook in Sec. V.

II. DIMENSION REDUCTION SCHEME BASED ON PARTIAL NORMAL FORM THEORY

Here we describe our procedure to scrutinize the internal structure and the effective dimension of phase space in terms of partial normal form theory. First, by introducing normal mode coordinates at the saddle point, the quadratic part $H_0^{(0)}$ of the n-DOF Hamiltonian becomes

$$H_0^{(0)} = \frac{\lambda}{2}\{(p_1^r)^2 - (q_1^r)^2\} + \sum_{\ell=2}^{n} \frac{\omega_\ell}{2}\{(p_\ell^r)^2 + (q_\ell^r)^2\} \quad (2.1)$$

$$= \lambda q_1^c p_1^c + \sum_{\ell=2}^{n} i\omega_\ell q_\ell^c p_\ell^c. \quad (2.2)$$

In this equation, $i\lambda$ is the imaginary frequency of the reactive mode, and ω_ℓ's $(\ell=2,\ldots,n)$ are the (real) frequencies of the bath modes. $q_\ell^r, p_\ell^r, q_\ell^c, p_\ell^c$ $(\ell=1,\ldots,n)$ are real and complex-valued normal mode coordinates and momenta. Their relations are

$$q_1^c = \frac{q_1^r + p_1^r}{2^{1/2}}, \quad p_1^c = \frac{p_1^r - q_1^r}{2^{1/2}}, \quad (2.3)$$

$$q_\ell^c = \frac{q_\ell^r - ip_\ell^r}{2^{1/2}}, \quad p_\ell^c = \frac{p_\ell^r - iq_\ell^r}{2^{1/2}} \quad (\ell = 2, \ldots, n). \quad (2.4)$$

We have defined mode 1 as the reactive mode and modes $2,\ldots,n$ as the bath modes. The action variables for the harmonic approximation are defined as $I_1 \equiv q_1^c p_1^c$ and $I_\ell \equiv iq_\ell^c p_\ell^c$.

The true Hamiltonian contains terms of order 3 and higher in addition to those in Eq. (2.2). We transform the Hamiltonian using a new set of variables $(\bar{\boldsymbol{q}}^c, \bar{\boldsymbol{p}}^c)$, which are called NF coordinates, to reduce the number of the coupling terms in the Hamiltonian when expressed in these new coordinates. After the NF transformation, the Hamiltonian is expressed in the polynomial of $(\bar{\boldsymbol{q}}^c, \bar{\boldsymbol{p}}^c)$. This new Hamiltonian is denoted as $\bar{H}(\bar{\boldsymbol{q}}^c, \bar{\boldsymbol{p}}^c)$. In the Hamiltonian, the off-diagonal terms, that is, terms with different powers of $\bar{q}_\ell^c$ and $\bar{p}_\ell^c$, denote couplings among the modes. This can be seen as follows. If the transformed Hamiltonian $\bar{H}$ takes the following form:

$$\bar{H}(\bar{\boldsymbol{q}}^c, \bar{\boldsymbol{p}}^c) = \lambda \bar{q}_1^c \bar{p}_1^c + \sum_{\ell=2}^{n} i\omega_\ell \bar{q}_\ell^c \bar{p}_\ell^c + \sum_{\Sigma_\ell j_\ell \geq 2} \bar{a}_j^c \prod_{\ell=1}^{n} (\bar{q}_\ell^c \bar{p}_\ell^c)^{j_\ell}, \quad (2.5)$$

where $\bar{a}_j^c$'s are the coefficients of the polynomial, then all of the new action variables $\bar{I}_1 = \bar{q}_1^c \bar{p}_1^c$, and $\bar{I}_\ell = i\bar{q}_\ell^c \bar{p}_\ell^c$ $(\ell = 2,\ldots,n)$ are constants of motion and the system is fully integrable. The Hamiltonian $\bar{H}$ of the form (2.5) is called a full normal form.

The NF transformation from $(\boldsymbol{q}^c, \boldsymbol{p}^c)$ to $(\bar{\boldsymbol{q}}^c, \bar{\boldsymbol{p}}^c)$ is constructed by a Lie perturbation theory [30]. We follow the formulation by Dragt and Finn [31]. We start by writing the Hamiltonian in a power series of a small parameter ϵ,

$$H(\boldsymbol{q}^c, \boldsymbol{p}^c, \epsilon) = \sum_{\nu=0}^{\infty} \epsilon^\nu H_\nu^{(0)}(\boldsymbol{q}^c, \boldsymbol{p}^c), \quad (2.6)$$

where $H_0^{(0)}$ is the harmonic part of the Hamiltonian [Eq. (2.2)]. To introduce a small parameter, we scale the coordinates $(\boldsymbol{q}^c, \boldsymbol{p}^c) \mapsto (\epsilon \boldsymbol{q}^c, \epsilon \boldsymbol{p}^c)$ and $H \mapsto \epsilon^{-2} H$. After the transformation is constructed, the parameter ϵ is set equal to 1. The canonical transformation $(\boldsymbol{q}^c, \boldsymbol{p}^c) \mapsto (\bar{\boldsymbol{q}}^c, \bar{\boldsymbol{p}}^c)$ is constructed by successive operations of Lie transformations,

$$\bar{q}_\ell = \exp(-\epsilon F_1)\exp(-\epsilon^2 F_2)\cdots\exp(-\epsilon^N F_N) q_\ell, \quad (2.7)$$

$$\bar{p}_\ell = \exp(-\epsilon F_1)\exp(-\epsilon^2 F_2)\cdots\exp(-\epsilon^N F_N) p_\ell, \quad (2.8)$$

where N is the order of the perturbation and $F_\nu (\nu = 1,\ldots,N)$ is an operation of the Poisson bracket with a function f_ν,

$$F_\nu = \{\cdot, f_\nu\}. \quad (2.9)$$

Then, the transformation of the Hamiltonian $H(\boldsymbol{q}^c, \boldsymbol{p}^c, \epsilon) \mapsto \bar{H}(\bar{\boldsymbol{q}}^c, \bar{\boldsymbol{p}}^c, \epsilon)$ is given by

$$\bar{H} = \exp(\epsilon^N F_N)\cdots\exp(\epsilon^2 F_2)\exp(\epsilon F_1) H. \quad (2.10)$$

If we define $\bar{H}^{(\mu)}(\bar{\boldsymbol{q}}^c, \bar{\boldsymbol{p}}^c, \epsilon)$ and $\bar{H}_\nu^{(\mu)}(\bar{\boldsymbol{q}}^c, \bar{\boldsymbol{p}}^c)$ by

$$\bar{H}^{(\mu)} = \exp(\epsilon^\mu F_\mu)\bar{H}^{(\mu-1)}$$
$$= \exp(\epsilon^\mu F_\mu)\cdots\exp(\epsilon^2 F_2)\exp(\epsilon F_1) H, \quad (2.11)$$

$$\bar{H}^{(\mu)} = \sum_{\nu=0}^{\infty} \epsilon^\nu \bar{H}_\nu^{(\mu)}, \quad (2.12)$$

we can readily obtain the following recursion formulas for $\bar{H}_\nu^{(\mu)}$:

$$\nu < \mu: \quad \bar{H}_\nu^{(\mu)} = \bar{H}_\nu^{(\mu-1)}, \tag{2.13}$$

$$\nu = \mu: \quad \bar{H}_\mu^{(\mu)} = \bar{H}_\mu^{(\mu-1)} + F_\mu \bar{H}_0^{(0)}, \tag{2.14}$$

$$\nu > \mu: \quad \bar{H}_\nu^{(\mu)} = \bar{H}_\nu^{(\mu-1)} + \sum_{s=1}^{\infty} \frac{(F_\mu)^s}{s!} \bar{H}_{\nu-s\mu}^{(\mu-1)}. \tag{2.15}$$

In the final Hamiltonian $\bar{H}=\bar{H}^{(N)}=\Sigma_{\nu=0}^{\infty}\epsilon^\nu \bar{H}_\nu^{(N)}$, the terms of the order ν are

$$\bar{H}_\nu^{(N)} = \bar{H}_\nu^{(N-1)} = \cdots = \bar{H}_\nu^{(\nu)} = \bar{H}_\nu^{(\nu-1)} + F_\nu \bar{H}_0^{(0)}, \tag{2.16}$$

because of Eqs. (2.13) and (2.14). Thus, F_ν can be determined so that the function $\bar{H}_\nu^{(N)}$ has a "desired" form.

In the present case, $\bar{H}_\nu^{(\nu-1)}$ is expressed in the form of a polynomial,

$$\bar{H}_\nu^{(\nu-1)}(\boldsymbol{q}^c,\boldsymbol{p}^c) = \sum_{\Sigma_\ell(j_\ell+k_\ell)=\nu+2} \alpha_{\boldsymbol{jk}}^{(\nu)} \prod_{\ell=1}^{n} (q_\ell^c)^{j_\ell}(p_\ell^c)^{k_\ell}, \tag{2.17}$$

where $\alpha_{\boldsymbol{jk}}^{(\nu)}$ is the coefficient of the polynomial. Moreover, $F_\nu \bar{H}_0^{(0)}=\{\bar{H}_0^{(0)},f_\nu\}$ and $\bar{H}_0^{(0)}=H_0^{(0)}$ has the form of Eq. (2.2). Therefore, if we are to eliminate the terms with certain values of $(\boldsymbol{j},\boldsymbol{k})$ from the final Hamiltonian $\bar{H}$, we set

$$f_\nu = \sum_{(\boldsymbol{j},\boldsymbol{k})} \frac{\alpha_{\boldsymbol{jk}}^{(\nu)}}{\gamma_{\boldsymbol{jk}}} \prod_{\ell=1}^{n} (q_\ell^c)^{j_\ell}(p_\ell^c)^{k_\ell}, \tag{2.18}$$

where the divisor $\gamma_{\boldsymbol{jk}}$ is defined as follows:

$$\gamma_{\boldsymbol{jk}} = \lambda(j_1-k_1) + i\sum_{\ell=2}^{n} \omega_\ell (j_\ell - k_\ell). \tag{2.19}$$

To obtain a well-defined transformation, the range of the summation in Eq. (2.18) is determined so that the polynomial series converges. If we have $\gamma_{\boldsymbol{jk}} \approx 0$ for certain combinations of $(\boldsymbol{j},\boldsymbol{k})$, then the corresponding coefficients of Eq. (2.18) take large values and cause the divergence of the series. This is the notorious problem of small divisors [32]. This situation arises when the bath mode frequencies $\omega_2,\ldots,\omega_n$ are nearly in the ratio of integers and is called the "resonance" effect. Such values of $(\boldsymbol{j},\boldsymbol{k})$ cannot be included in the summation of Eq. (2.18) and have to be kept in $\bar{H}$. Which terms should be included in $\bar{H}$ must be determined based on convergence of the transformed Hamiltonian.

In previous works [13–25], it was found that the reactive DOF can be separated from all the bath modes even when the couplings among the bath modes wash out all the invariants of motion in the bath space. As pointed out previously [11] this is due to the fact that resonance conditions, which cause divergence in perturbation expansion through the problem of small divisors, can never be satisfied between real and imaginary frequencies [33]. For the purpose of extracting phase-space objects such as no-return transition state and NHIM, the separation of the reactive mode from the bath space is sufficient, which yields the following NF Hamiltonian [24,25]:

$$\bar{H} = \lambda \bar{q}_1^c \bar{p}_1^c + \sum_{\ell=2}^{n} i\omega_\ell \bar{q}_\ell^c \bar{p}_\ell^c + \sum_{\Sigma_\ell j_\ell \geq 2} \bar{a}_{\boldsymbol{j}}^c \prod_{\ell=1}^{n} (\bar{q}_\ell^c \bar{p}_\ell^c)^{j_\ell} + \sum_{j_1=k_1} \bar{a}_{\boldsymbol{jk}}^c \prod_{\ell=1}^{n} (\bar{q}_\ell^c)^{j_\ell}(\bar{p}_\ell^c)^{k_\ell}, \tag{2.20}$$

where $\bar{a}_{\boldsymbol{j}}^c$'s and $\bar{a}_{\boldsymbol{jk}}^c$'s are the coefficients of the diagonal and the off-diagonal terms, respectively. Note that Eq. (2.20) does not include terms with $j_1 \neq k_1$ although it includes all the coupling terms among the bath modes. This leads us to expect that, up to moderately high energy above the reaction threshold, the action $\bar{I}_1=\bar{q}_1^c\bar{p}_1^c$ of the reactive mode can persist as an approximate constant. Therefore the reactive mode is separated from the bath space [24,25].

However, for the $n(>3)$-DOF systems, even after the separation of the reactive mode the NHIM is still a high-dimensional abstract object such that the corresponding invisible SOS is not helpful in clarifying the phase-space structure of the NHIM. Thus it is desirable to include as few terms as possible in $\bar{H}$, because the bath mode dynamics can be simplified with a small number of coupling terms among the bath modes.

In this paper, we present the further reduction of the Hamiltonian represented by the following form:

$$\bar{H} = \lambda \bar{q}_1^c \bar{p}_1^c + \sum_{\ell=2}^{n} i\omega_\ell \bar{q}_\ell^c \bar{p}_\ell^c + \sum_{\Sigma_\ell j_\ell \geq 2} \bar{a}_{\boldsymbol{j}}^c \prod_{\ell=1}^{n} (\bar{q}_\ell^c \bar{p}_\ell^c)^{j_\ell} + \sum_{\boldsymbol{d}} \sum_{(\boldsymbol{j}-\boldsymbol{k})\propto\boldsymbol{d}} \bar{a}_{\boldsymbol{jk}}^c \prod_{\ell=1}^{n} (\bar{q}_\ell^c)^{j_\ell}(\bar{p}_\ell^c)^{k_\ell}, \tag{2.21}$$

which includes only those terms with $(\boldsymbol{j}-\boldsymbol{k})\propto\boldsymbol{d}$, where the integer vector $\boldsymbol{d}=(d_1,d_2,\ldots,d_n)$ covers all the terms which cannot be eliminated. If $\boldsymbol{d}$ covers all the value of $\boldsymbol{d}=(0,d_2,\ldots,d_n)$ with $d_1=0$, one can obtain Eq. (2.20).

To examine which terms can be eliminated from $\bar{H}$ or must be included, we use the energy error [23] $\Delta E^{(N)}=|\bar{H}^{(N)}-H|$ as a criterion of the convergence, where $\bar{H}^{(N)}$ is the NF Hamiltonian up to the Nth order and H is the true Hamiltonian. Note that, even with the off-diagonal terms, the form (2.21) is simpler than the form (2.20), because the number of terms in Eq. (2.21) is restricted by the condition $(\boldsymbol{j}-\boldsymbol{k})\propto\boldsymbol{d}$. Hereinafter we call the forms like Eq. (2.20) and Eq. (2.21) a "partial NF" (PNF) in contrast to the full NF.

With the reduced number of the coupling terms, we can examine the value of each term along the trajectories. Depending on the system, it can happen that some of the terms have negligibly small values. Then, we can further restrict the range of $\boldsymbol{d}$ in Eq. (2.21) by ignoring those small terms. If the range of the summation covers only those terms with $d_1=d_2=\cdots=d_m=0$ for some $m<n$, the resulting Hamiltonian takes the following form:

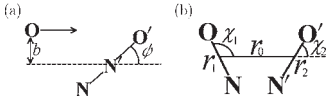

FIG. 2. Definition of the parameters used in this paper. (a) Impact parameter b and the initial orientation ψ of N_2O. (b) Jacobi coordinates.

$$\bar{H} = \lambda \bar{q}_1^c \bar{p}_1^c + \sum_{\ell=2}^{n} i\omega_\ell \bar{q}_\ell^c \bar{p}_\ell^c + \sum_{\Sigma_\ell j_\ell \geq 2} \bar{a}_j^c \prod_{\ell=1}^{n} (\bar{q}_\ell^c \bar{p}_\ell^c)^{j_\ell} + \sum_{j,k} \bar{a}_{jk}^c \left\{ \prod_{\ell=1}^{m} (\bar{q}_\ell^c \bar{p}_\ell^c)^{k_\ell} \right\} \left\{ \prod_{\ell=m+1}^{n} (\bar{q}_\ell^c)^{j_\ell} (\bar{p}_\ell^c)^{k_\ell} \right\}. \tag{2.22}$$

With this Hamiltonian, the actions for the modes $1,2,\ldots,m$ are constants of motion. Thus, we can separate these modes and there remain $(n-m)$ DOF to investigate. The effective Hamiltonian for these $(n-m)$ modes is given by

$$\begin{aligned} \bar{H}^{\mathrm{eff}}(\bar{q}_{m+1}^c, \ldots, \bar{q}_n^c, \bar{p}_{m+1}^c, \ldots, \bar{p}_n^c, \bar{I}_1, \ldots, \bar{I}_m) &= \lambda \bar{I}_1 + \sum_{\ell=1}^{m} \omega_\ell \bar{I}_\ell + \sum_{\ell=m+1}^{n} i\omega_\ell \bar{q}_\ell^c \bar{p}_\ell^c \\ &+ \sum_{\Sigma_\ell j_\ell \geq 2} \bar{a}_j^c \left\{ \prod_{\ell=1}^{m} \bar{I}_\ell^{j_\ell} \right\} \left\{ \prod_{\ell=m+1}^{n} (\bar{q}_\ell^c \bar{p}_\ell^c)^{j_\ell} \right\} \\ &+ \sum_{j,k} \bar{a}_{jk}^c \left\{ \prod_{\ell=1}^{m} (\bar{I}_\ell)^{k_\ell} \right\} \left\{ \prod_{\ell=m+1}^{n} (\bar{q}_\ell^c)^{j_\ell} (\bar{p}_\ell^c)^{k_\ell} \right\}, \end{aligned} \tag{2.23}$$

with $\bar{I}_1 = \bar{q}_1^c \bar{p}_1^c$ and $\bar{I}_\ell = i\bar{q}_\ell^c \bar{p}_\ell^c (\ell = 2,\ldots,m)$ appearing as constant parameters. This completes our dimension reduction from an n-DOF system to an effective $(n-m)$-DOF system.

III. MODEL AND CALCULATION

A. Description of path 1 trajectories

Here we describe the model system to which we apply PNF analyses in this paper. Throughout the paper, we adopt the nuclear masses of $^{18}O(^1D) + {}^{14}N{}^{14}N{}^{16}O$ for which the experiment [34] and the calculation [28] have been done. For the sake of brevity we fix the initial rovibrational energy of N_2O to zero and the impact parameter b [see Fig. 2(a)] is confined to zero. It was found that freezing the initial motion of N_2O does not change the product vibrational distribution significantly [28] and also, as will be shown below, one can find significant vibrational excitation of the old NO for $b=0$. Therefore the analysis of the motion with $b=0$ can be regarded as a first important step for understanding the energy exchange in this system. The numerical simulation of the trajectories is performed by numerically integrating the equations of motion for the Jacobi vectors by the fourth-order Runge-Kutta method with variable time steps [35].

To describe the trajectories, we plot the time evolution of Jacobi coordinates $(r_0, r_1, r_2, \chi_1, \chi_2)$ as defined in Fig. 2(b). We denote the internuclear distances of NO and N′O′ moieties as r_1 and r_2, respectively. The distance between the mass centers of the two NO's is denoted by r_0. χ_1 and χ_2 are the angles between the line connecting the mass centers of NO's and the nuclear axes of NO and N′O′, respectively. The time evolution of the Jacobi coordinates is shown in the upper panels of Figs. 3(a)–3(d) for four different initial orientations ψ of N_2O, where ψ is defined in Fig. 2(a). The initial conditions are generated as follows: At $t=0$, the $O(^1D)$ atom is placed in the distance of 8 Å from the mass center of N_2O with the impact parameter $b=0$ and the translational energy 20.9 kJ/mol $=3.47\times10^{-20}$ J, which corresponds to the experimental condition of Ref. [34]. N_2O is placed with the orientation $\psi = 0°, 5°, 10°$, and 13° for panels (a), (b), (c), and (d) of Fig. 3, respectively. Note that, for $b=0$, the trajectories of path 1 cover the range of $|\psi| \approx 0$–15° (see Fig. 6 of Ref. [28]), and that there is a symmetry with respect to the reflection $\psi \mapsto -\psi$ so that we have only to consider the trajectories of $\psi = 0$–15°. The trajectory of $\psi=0$ has an exactly collinear configuration and thus experiences no force along the bending direction because of the symmetry. The other trajectories of path 1, that is, the trajectories of $\psi \neq 0$ start with near-collinear configurations $(\chi_1 \approx \pi, \chi_2 \approx 0)$. After they pass by the regions near the collinear saddle, they fall into *trans*-type configurations $(\chi_1 < \pi, \chi_2 < 0)$. Thus, in the early stage of the reaction, that is, when the system is in near-collinear configurations, the motion can be well approximated by the motion for $\psi=0$.

B. Taylor expansion of the Hamiltonian around the collinear saddle point

Here we perform the Taylor expansion of the Hamiltonian around the collinear saddle point (*Is*). This saddle point connects two *trans*-shaped minima (*Tm*),

$$\mathrm{O\!\!\diagdown N-N \diagdown\!\!O} \rightleftharpoons \mathrm{O\!\!\diagup N-N \diagup\!\!O}. \tag{3.1}$$

These two minimum configurations can be distinguished from each other in the planar system, although only one of them is shown in Fig. 1. As was shown in Ref. [28], trajectories go downhill along a bath mode direction of *Is* until they pass by the region near *Is*, and then fall into either *Tm* following the reactive mode at *Is*.

We obtain the expansion coefficients of the potential function by calculating the Lagrange interpolation polynomial [35] with potential energy values at grid points around *Is*, while the analytic expansion form for the kinetic term can be obtained straightforwardly. In the lower panels of Figs. 3(a)–3(d), the error $\Delta V^{(n)} = V^{(n)} - V$ of the nth-order polynomial approximation for the potential is shown for each initial condition, where $V^{(n)}$ denotes the nth-order polynomial expansion and V is the true value of the potential. If the error is small, it means that the system is in the vicinity of the saddle point. In order to judge whether the error is small or not, it must be compared with the typical energy per one degree of freedom, which is of the order of 10^{-19} J for this system. For

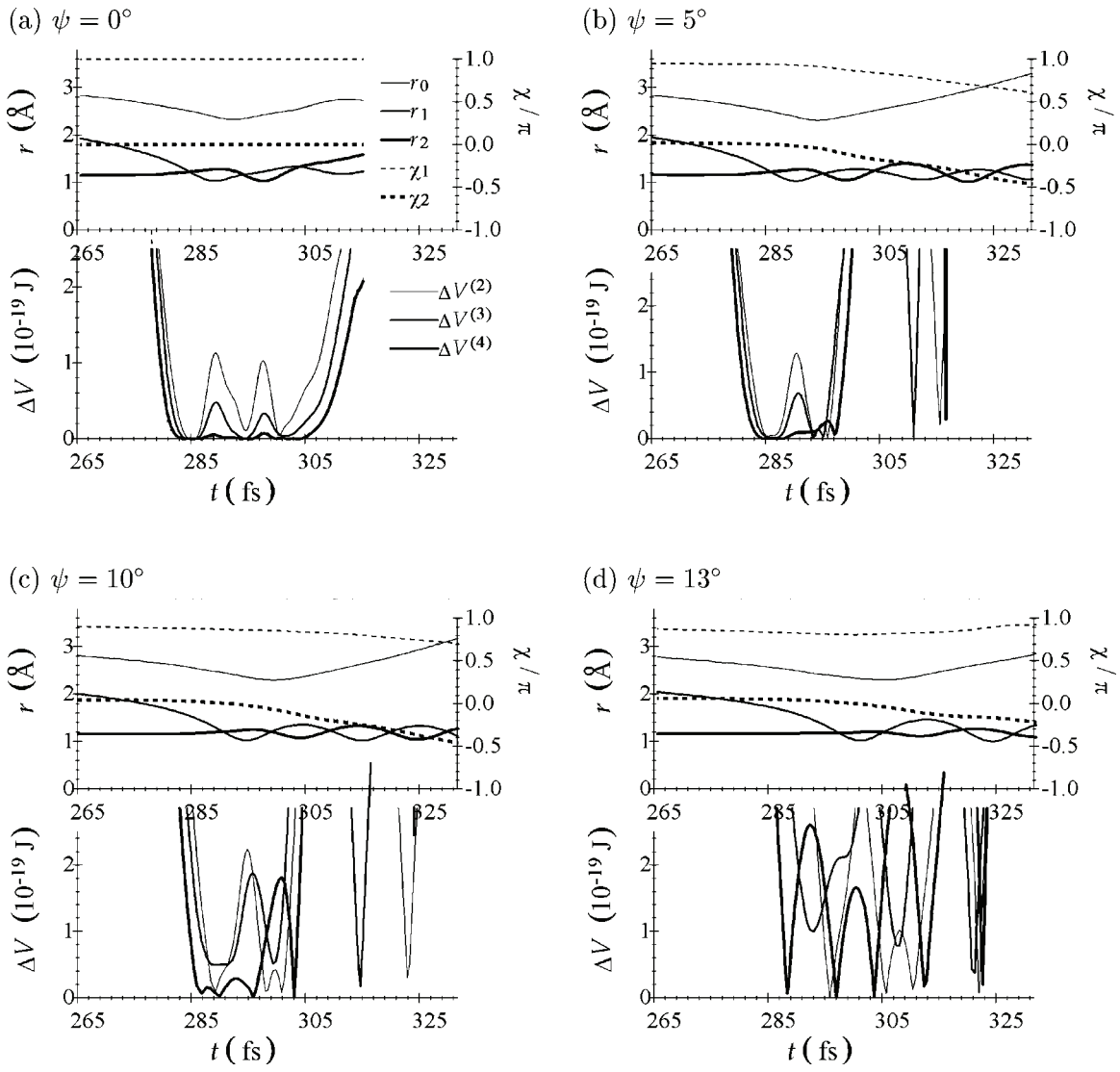

FIG. 3. Time evolution of Jacobi coordinates and the residual error of Taylor expansion of the potential energy shown for four different initial conditions of ψ. Upper panels: Time evolution of r_0 (thin solid line), r_1 (medium solid line), r_2 (thick solid line), χ_1 (thin dotted line), and χ_2 (thick dotted line). Lower panels: Residual error of Taylor expansion up to the second (thin line), third (medium line), and fourth order (thick line).

the trajectory of $\psi=0$ [Fig. 3(a)], the error $\Delta V^{(4)}$ is one order of magnitude smaller than this value in the time range of $t \approx 280-305$ fs. For $\psi=5°$ and 10°, the time range for $\Delta V^{(4)} \leq 10^{-20}$ is $t \approx 283-293$ fs, and $t \approx 287-291$ fs, respectively. Thus, the trajectories of $\psi \leq 10°$ come sufficiently close to the collinear saddle point. The trajectories of $\psi \leq 10°$ cover 2/3 of the whole path 1 trajectories. This means that a significant proportion of the path 1 trajectories approach the collinear saddle point. Moreover, the excitation of the old NO, r_2, begins when the system comes close to the saddle point. Thus, we focus below on the dynamics in the vicinity of *Is*.

C. The internal structure of the phase space at saddle *Is*

The displacements and the frequencies of the normal modes at the collinear saddle point are shown in Fig. 4. We define the reactive mode as mode 1, and the bath modes are numbered in the decreasing order of their frequencies. The normal mode coordinates $(\boldsymbol{q}^c, \boldsymbol{p}^c)$ are constructed as linear combinations of the displacements of the Jacobi coordinates, and are used as the starting coordinates of the PNF procedure.

By examining the energy error, we have found that the terms listed in Table I should be kept in the transformed Hamiltonian, since their elimination results in a larger error $\Delta E^{(4)}$ than the error $\Delta E^{(2)}$ of the harmonic approximation. The integer vector $\boldsymbol{d}$ in Eq. (2.21) covers all the terms listed in Table I. Even with the off-diagonal terms, the form of $\bar{H}$ is still much simpler than the original form. Namely, a fourth-order polynomial with ten variables has 1001 terms, whereas there are only 12 types (listed in Table I) of coupling terms in Eq. (2.21).

TABLE I. Types of the terms that cannot be eliminated from the NF Hamiltonian. j_ℓ and k_ℓ are the exponents of $\bar{q}_\ell^c$ and $\bar{p}_\ell^c$ in $\bar{H}$ [see Eq. (2.21)].

(j_1-k_1):	(j_1-k_2):	(j_3-k_3):	(j_4-k_4):	(j_5-k_5)
0	1	0	−3	0
0	0	1	−1	0
0	1	−1	−2	0
0	0	0	0	2
0	0	0	2	−2
0	0	1	0	0
0	0	1	1	0
0	1	−2	0	0
0	0	1	−2	0
0	0	0	1	0
0	0	2	−1	0
0	0	2	1	0

Note that all of the terms listed in Table I have zero in their first component. Therefore $\bar{I}_1=\bar{q}_1^c\bar{p}_1^c$ is a local constant of motion. This means that the motion along mode 1 is separable from the others. Similar situations are found in former studies [13–19,21,22,24,36,37]. It is attributed to the fact that there can be no resonance between imaginary and real frequencies [33]. Note also that Table I contains those terms for which all $(j_\ell-k_\ell)$'s are non-negative, such as 0:0:1:0:0 and 0:0:2:1:0. These terms are not of the "resonance" type but cannot be eliminated from the PNF Hamiltonian. This might arise from the fact that the values of the actions for models 3 and 4 are so large that they cannot be eliminated by perturbation.

IV. ANALYSES OF THE DYNAMICS

A. Evaluation of the couplings

First, we analyze the time development of the vibrational energy of each of the PNF coordinates. The upper panels of Fig. 5 show the values of $\omega_\ell\bar{I}_\ell$, that is, a rough estimate of the vibrational energy of each mode, calculated along the trajectories shown in Fig. 3. The lower panels of the same figure show the energy errors of the harmonic (thin dotted lines) and the PNF (thick solid lines) Hamiltonian, respectively. Here we can see that, for $\psi\leq 10°$, the PNF shows convergence for the time region in which trajectories are in the vicinity of the saddle point (when compared with Fig. 3). Moreover, the action value for mode 1 is nearly constant, as can be predicted from the PNF Hamiltonian [Eq. (2.21) and Table I].

Now, we introduce the concept of NHIM. The NHIM is defined in terms of $(\bar{\boldsymbol{q}}^c,\bar{\boldsymbol{p}}^c)$ as

$$\mathcal{M}_{\mathrm{NHIM}}=\{(\bar{p}_1^c,\ldots,\bar{p}_5^c,\bar{q}_1^c,\ldots,\bar{q}_5^c)|\bar{p}_1^c=\bar{q}_1^c=0;$$

$$\bar{H}(\bar{I}_1=0,\bar{q}_2^c,\bar{q}_3^c,\bar{q}_4^c,\bar{q}_5^c,\bar{p}_2^c,\bar{p}_3^c,\bar{p}_4^c,\bar{p}_5^c)=E\}, \tag{4.1}$$

at a given energy E. Because the reactive degree of freedom is decoupled from the bath space in the $(\bar{\boldsymbol{q}}^c,\bar{\boldsymbol{p}}^c)$ coordinate system, the NHIM forms an invariant set.

Note that the trajectories of $\psi\leq 10°$ have qualitatively similar properties to each other as seen in Figs. 3 and 5. This can be understood based on the fact that in the vicinity of the saddle, the motions along and normal to NHIM are separated from each other. Therefore, we now focus on the case of $\psi=0$ to extract the underlying mechanism of the energy transfer. For $\psi=0$, we can treat the system locally as an effective three-DOF system with an effective Hamiltonian given by

$$H^{\mathrm{eff}}(\bar{q}_2^c,\bar{q}_3^c,\bar{q}_4^c,\bar{p}_2^c,\bar{p}_3^c,\bar{p}_4^c)=\bar{H}(\bar{q}_1^c=0,\bar{q}_2^c,\bar{q}_3^c,\bar{q}_4^c,\bar{q}_5^c=0,\bar{p}_1^c=0,\bar{p}_2^c,\bar{p}_3^c,\bar{p}_4^c,\bar{p}_5^c=0), \tag{4.2}$$

when the system is in the neighborhood of the collinear saddle *Is*. The dynamics of H^{eff} takes place in a subspace of the NHIM.

We further simplify the above Hamiltonian by taking into account the coupling terms listed in Table I. In order to assess their effects, we have plotted, in Fig. 6, the values of these terms along the trajectory of $\psi=0$. Among the coupling terms including mode 2, only the "0:1:−2:0:0" term is non-negligible, but it is still smaller than the coupling terms between modes 3 and 4. Thus, modes 3 and 4 have large anharmonicity and are strongly coupled with each other, whereas mode 2 is coupled only weakly with mode 3 through one term. Therefore we can gain more insight into the dynamics by making the following separation of the Hamiltonian:

$$H^{\mathrm{eff}}(\bar{q}_2^c,\bar{q}_3^c,\bar{q}_4^c,\bar{p}_2^c,\bar{p}_3^c,\bar{p}_4^c)=\bar{H}_{34}(\bar{q}_3^c,\bar{q}_4^c,\bar{p}_3^c,\bar{p}_4^c)+\omega_2\bar{I}_2+\sum\bar{a}_{jk}^c\prod_{\ell=2}^{4}(\bar{q}_\ell^c)^{j_\ell}(\bar{p}_\ell^c)^{k_\ell}, \tag{4.3}$$

where $\bar{H}_{34}(\bar{q}_3^c,\bar{q}_4^c,\bar{p}_3^c,\bar{p}_4^c)=H^{\mathrm{eff}}(\bar{q}_2^c=0,\bar{q}_3^c,\bar{q}_4^c,\bar{p}_2^c=0,\bar{p}_3^c,\bar{p}_4^c)$. The first term can be interpreted as a Hamiltonian of a two-DOF subsystem consisting of modes 3 and 4, the second is the harmonic energy of mode 2, and the third denotes the coupling between the two-DOF subsystem and mode 2. When we plot the values of $\bar{H}_{34}$ and $\omega_2\bar{I}_2$ as functions of time, a gradual and monotonic decrease of $\bar{H}_{34}$ and an increase of $\bar{I}_2$ were found. This is consistent with the idea presented above, that is, the coupling between mode 2 and the two-DOF subsystem is due to only one resonance term.

We now look deeply into this two-DOF subsystem in the next subsection.

B. Dynamics of the two-DOF subsystem

Figure 7(a) shows the SOS of the two-DOF Hamiltonian $\bar{H}_{34}$ for $\bar{q}_4^r=0, \bar{p}_4^r>0$ with the horizontal and vertical axes being $\bar{q}_3^r$ and $\bar{p}_3^r$, respectively. The value of the Hamiltonian $\bar{H}_{34}$, i.e., the energy of these trajectories, is chosen as follows: After calculating the trajectory of $\psi=0$ by the original Hamiltonian up to $t=283$ fs, we transform the coordinates to $(\bar{\boldsymbol{q}}^r, \bar{\boldsymbol{p}}^r)$. Substituting their values into the Hamiltonian $\bar{H}_{34}$, we obtain the value of $\bar{H}_{34}$.

In Fig. 7(a), we can see the existence of regular tori in the outer region, whereas the inner region shows irregular behavior. To find which region corresponds to the actual reaction trajectories, we have plotted, in Fig. 7(b), the SOS for five trajectories. The initial conditions of these five trajectories are chosen as follows. First, we calculate the trajectory of $\psi=0$ using the original Hamiltonian up to five different times $t=283,290,295,300$, and 305 fs. They cover the time interval where the system stays near the saddle [see Fig. 5(a)]. The values of the Jacobi coordinates and their conjugate momenta at these five instances are transformed to the values of $(\bar{\boldsymbol{q}}^r, \bar{\boldsymbol{p}}^r)$ to give the five initial conditions $(\bar{q}_3^r, \bar{q}_4^r, \bar{p}_3^r, \bar{p}_4^r)$.

In Fig. 7(b), the system first appears in the intermediate region between the center and the outermost ellipse. This is because the reaction trajectories start with an elongation of the new NO bond, which corresponds to simultaneous excitation of the symmetric and antisymmetric stretches. At early times, the system is found in the region of regular torus structure. Then the torus shrinks as the time passes, due to the coupling with mode 2, and finally enters into the inner irregular region after $t=290$ fs.

The tori found in the early time period are topologically the same as those of the harmonic case $[(\bar{q}_3^r)^2+(\bar{p}_3^r)^2=\text{const.}]$. Strictly speaking, their shapes are distorted from the true circle. We should also note that the coordinates used in Fig. 7 are the PNF coordinates, whose main parts are the normal mode coordinates but they are not exactly the same. However, bifurcation into the local modes [1–4] or other types of periodic orbits [5–10] does not occur for this system (at least in the region corresponding to the reaction trajectories). Hereafter, we refer to this motion as "distorted normal mode."

So far we have limited our attention to the trajectory of $\psi=0$, which is collinear and thus contained in the NHIM. This is based on the idea that the deviation from $\psi=0$ mainly results in the displacement in the direction of the reactive mode (mode 1), which has little effect on the bath mode dynamics. However, its effect on the bath modes is not exactly zero and thus it is worth investigating whether it is really negligible. This is performed by taking the initial value of $(\bar{q}_3^r, \bar{q}_4^r, \bar{p}_3^r, \bar{p}_4^r)$ from trajectories of $\psi\neq 0$. Although not shown in figures, we have also found a distorted normal- mode type structure with the initial condition taken at $t=285,290$ fs for $\psi=5°$, and $t=290$ fs for $\psi=10°$. The chaotic motion in the inner region does not appear for these trajectories. This is because their residence times in the vicinity of the saddle point are finite, whereas the collinear trajectory $(\psi=0)$ remains in the NHIM all the time. Thus, the noncollinear trajectories do not have enough time to travel into the inner region. Therefore we can conclude that the distorted normal mode picture holds for the noncollinear trajectories when they enter into the vicinity of the saddle point.

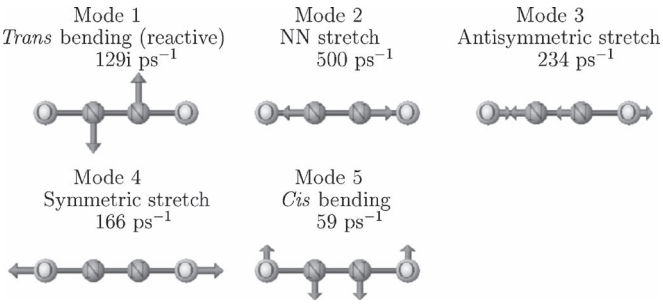

FIG. 4. Normal modes at the collinear saddle point.

C. Mechanism of efficient energy transfer

Here we propose a simple model to explain the efficient energy transfer in spite of short lifetime in terms of the geometrical feature of the phase space in the region of saddle *Is*. Qualitatively, the symmetric $(\bar{q}_4^r)$ and antisymmetric $(\bar{q}_3^r)$ coordinates can be expressed as

$$\bar{q}_4^r \approx q_4^r \sim \frac{\delta r_1 + \delta r_2}{2^{1/2}}, \quad \bar{q}_3^r \approx q_3^r \sim \frac{\delta r_1 - \delta r_2}{2^{1/2}}, \tag{4.4}$$

respectively, where δr_1 and δr_2 are the deviation of the bond length of the new and old NO, respectively, from their equilibrium values. Since the normal mode picture is conserved with a little distortion, the time evolution of $\bar{q}_4^r$ and $\bar{q}_3^r$ is approximated by simple trigonometric functions,

$$\bar{q}_4^r \approx A\cos(\omega_4 t), \quad \bar{q}_3^r \approx A\cos(\omega_3 t), \tag{4.5}$$

Thus, the vibrations of the new and old NO bonds are

$$\delta r_1 \sim \frac{q_4^r + q_3^r}{2^{1/2}} \approx 2^{-1/2}A[\cos(\omega_4 t) + \cos(\omega_3 t)]$$
$$= 2^{1/2}A\cos\left(\frac{\omega_4 - \omega_3}{2}t\right)\cos\left(\frac{\omega_4 + \omega_3}{2}t\right), \tag{4.6}$$

$$\delta r_2 \sim \frac{q_4^r - q_3^r}{2^{1/2}} \approx 2^{-1/2}A[\cos(\omega_4 t) - \cos(\omega_3 t)]$$
$$= 2^{1/2}A\sin\left(\frac{\omega_4 - \omega_3}{2}t\right)\sin\left(\frac{\omega_4 + \omega_3}{2}t\right). \tag{4.7}$$

The interpretation of the right-hand sides are that they are oscillating with the mean frequency $(\omega_4+\omega_3)/2$ while their amplitudes vary with the frequency $(\omega_4-\omega_3)/2$. This change of the amplitudes is called "beat." The time scale for the excitation of the old NO bond can be estimated by $\pi/2(\omega_4-\omega_3)$. If we use the values shown in Fig. 4, it becomes 23 fs,

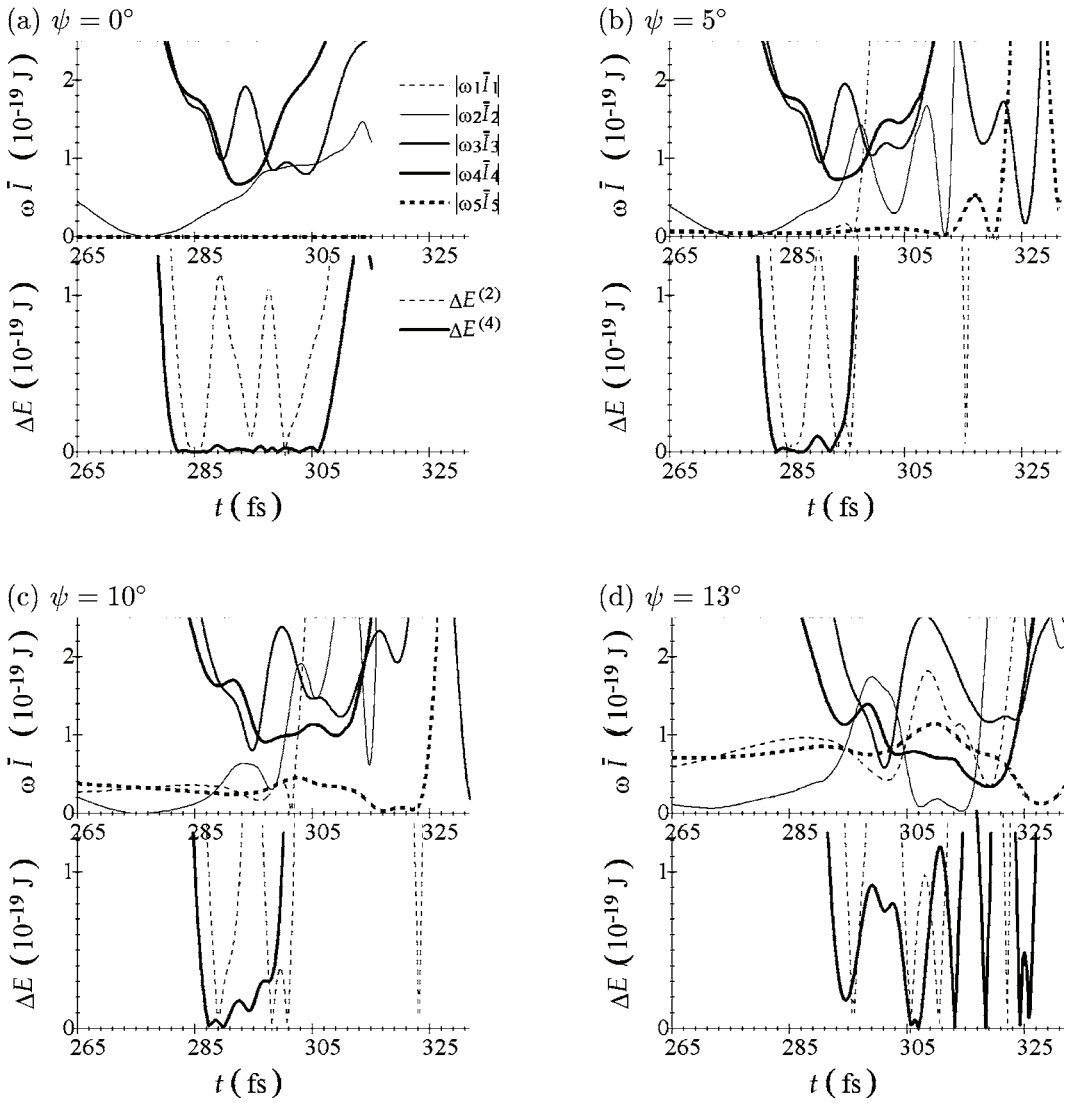

FIG. 5. Results of PNF calculation shown for the same four initial conditions as in Fig. 3. Upper panels: Time evolution of the actions multiplied by the harmonic frequencies. The values for modes 1, 2, 3, 4, and 5 are shown by thin dotted, thin solid, medium solid, thick solid, and thick dotted lines, respectively. Lower panels: Energy errors. The thin line depicts the difference $\Delta E^{(2)}$ between the true Hamiltonian and the harmonic approximation. The thick line depicts the difference $\Delta E^{(4)}$ between the true Hamiltonian and the fourth-order PNF Hamiltonian.

which is of the same order as the residence time in the vicinity of the collinear saddle point [see Figs. 3(a)–3(d)]. This means that the residence time is sufficient to allow the excitation of the old NO vibration. Here, the important point is that the energy transfer takes place very fast, since the period of the beat is short. Even though the lifetime of the reaction intermediate is short, the time scale of the beat is comparable to the lifetime of the reaction intermediate and thus causes a significant excitation of the old bond when the system passes through the saddle *Is*. The short time scale of the beat derives from the relatively large difference between the frequencies of the symmetric and antisymmetric stretches. Note also that the regularity is not strictly required for the beat model. Even in the case of chaos, it is possible that the system sees so-called "vague tori" [38,39] and follows a orbit similar to that of the distorted normal mode picture for some short time period. The important aspect is the existence of two different mechanisms for the energy transfer. One is the randomization by strong chaos, where the system travels around in the potential well. This is close to the traditional picture of the energy transfer, that is, the randomization after a long lifetime in a deep well. The other mechanism is the motion of the distorted normal mode type, where the system visits only a part of the phase space but the motion is represented as a superposition of a few distorted normal modes. If the periods of the beats are short enough, efficient energy transfer takes place. In particular, this mechanism works not only in the well but also near the saddle. As one of the possible mechanisms of the origin of efficient energy exchange of the reaction of $O(^1D)+N_2O \rightarrow NO+NO$, the present work analysis suggests the beat mechanism arisen from the preservation of the distorted normal mode picture in spite of the high energy near the saddle and the relatively large difference between

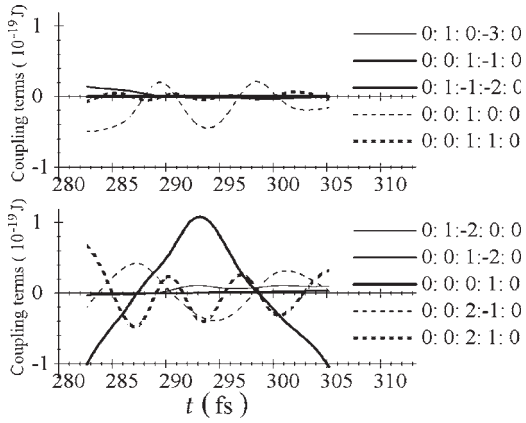

FIG. 6. Values of the coupling terms in the NF Hamiltonian as functions of time calculated for the trajectory of $\psi=0$.

the frequencies of the symmetric and antisymmetric stretches.

V. SUMMARY AND OUTLOOK

A new systematic dimension reduction scheme in the local region near a stationary point was proposed based on the partial normal form theory (PNF), which decomposes the multidimensional phase space into new building blocks of the invariants. The crux is the PNF scheme, which eliminates many coupling terms through coordinate transformations. By careful investigation of the coupling terms and a check of the convergence, we succeeded in eliminating not only the coupling between the reactive and bath modes, but also as many couplings as possible among the bath modes. Then, in PNF coordinates the number of the coupling terms in the Hamiltonian decreased drastically compared to the original coordinates. As an illustrative example, the dynamics of the short lifetime trajectories of a near-collinear approach, named "path 1," [28] of the reaction $O(^1D)+N_2O \rightarrow NO+NO$, was investigated. This reaction was found to exhibit a significant energy transfer from the new to the old NO vibration in spite of its short lifetime [28,34]. It was found that the symmetric and antisymmetric NO stretching modes were strongly coupled to each other, whereas the other modes were uncoupled or only weakly coupled to these modes. The dynamics in the vicinity of the saddle *Is* could be well reduced into a two-DOF system consisting of the two stretching modes.

Analyses of the two-DOF subsystem revealed the robust persistence of the distorted normal mode picture for the reaction trajectories in spite of high energy above the saddle point. The period of the beat between the two NO stretching modes was of the order of 10 fs, due to the large difference between their frequencies. This period is short enough to cause excitation of the old NO vibration. Thus we proposed a simple model to explain the efficient energy transfer from the new to the old NO in terms of the beat between the distorted normal mode pictures buried in the multidimensional phase space even at high energy above the saddle point. It should be noted, however, that for the comprehensive understanding of the mechanism of the reaction, it is of

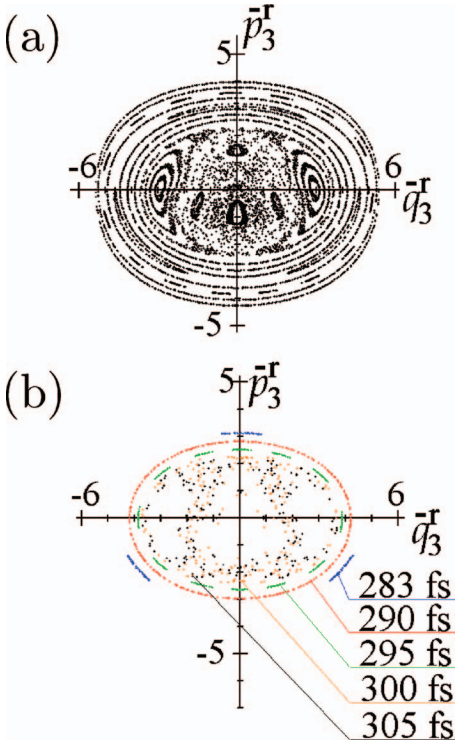

FIG. 7. (Color online) Poincaré surface of section for the two-DOF subsystem consisting of modes 3 and 4 calculated with the polynomial Hamiltonian $\bar{H}_{34}$. (a) Total Poincaré surface of section with $\bar{q}_4^r=0$ and $\bar{p}_4^r>0$ plotted with $\bar{q}_3^r$ and $\bar{p}_3^r$. The unit is 10^{-17} kg$^{1/2}$ ms$^{-1/2}$. The energy is $\bar{H}_{34}=3.50\times10^{-19}$ J corresponding to the value of $(\bar{q}_3^r,\bar{q}_4^r,\bar{p}_3^r,\bar{p}_4^r)$ at $t=283$ fs for the trajectory of $\psi=0$. (b) The Poincaré surface of section is drawn for five different initial values of $(\bar{q}_3^r,\bar{q}_4^r,\bar{p}_3^r,\bar{p}_4^r)$. The times from which the initial values were taken are $t=283$, 290, 295, 300, 305 fs and are indicated in the figure. The points for $t=300$ and 305 fs are distinguished by color: Light (or orange) and black color correspond to $t=300$ and 305 fs, respectively.

vital importance to extend the PNF analysis to the other stationary points and the other paths. In addition, although the planar model was found [28] to reproduce the essential feature of the experimentally observed distribution [34], it is also worthwhile to scrutinize the phase-space geometry of the nonplanar system by using the PNF analysis.

Our PNF method is generally applicable to any systems of many degrees of freedom and provides us with an essential clue of the underlying geometrical structure of the multidimensional phase space. For example, chemical reactions $O(^1D)+HCl$ [40–42], $O(^1D)+H_2O$ [43,44], and $H+NO_2$, [45–47] are also quite interesting systems because the PES have deep wells but the product state distributions deviate significantly from the statistical distributions (that is, they are counterintuitive). These require systematic scrutiny of the phase space in the region of a potential well. Our dimension reduction by PNF will be of great help to capture the phase-space properties of any stationary point. To be sure, it depends on the system to what extent we can reduce the dimension of the system. The Poincaré surface of section is a powerful tool only for the cases where the system can be

reduced to a two-DOF system. However, even if the system can only be reduced to an $m(\geq 3)$-DOF system, this makes the analyses much simpler than the original $n(>m)$-DOF system. Moreover, it is significant information by itself which modes are separated and which modes are strongly coupled to the other modes. This reveals a nonuniform character of the phase space highly contrasted to a simple statistical description where all the DOF are completely mixed. Thus, our PNF method is expected to capture the dynamical structure of the system and thereby shed light on the origin of complicated behavior in chemical reaction dynamics.

ACKNOWLEDGMENTS

This work is partially supported by JSPS, JST/CREST, Grant-in-Aid for research on priority area "Control of Molecules in Intense Laser Fields," MEXT, the 21st century COE of "Origin and Evolution of Planetary Systems (Kobe University)," MEXT, and by the discretionary research grant of university president for researchers of Nara Women's University.

[1] C. Jaffé and P. Brumer, J. Chem. Phys. **73**, 5646 (1980).
[2] E. L. Sibert III,W. P. Reinhardt, and J. T. Hynes, J. Chem. Phys. **77**, 3583 (1982).
[3] E. L. Sibert III, J. T. Hynes, and W. P. Reinhardt, J. Chem. Phys. **77**, 3595 (1982).
[4] M. S. Child and L. Halonen, Adv. Chem. Phys. **57**, 1 (1984).
[5] L. Xiao and M. E. Kellman, J. Chem. Phys. **93**, 5805 (1990).
[6] J. P. Rose and M. E. Kellman, J. Chem. Phys. **105**, 10743 (1996).
[7] Z.-M. Lu and M. E. Kellman, J. Chem. Phys. **107**, 1 (1997).
[8] J. Weiß, J. Hauschildt, S. Yu. Grebenshchikov, R. Düren, R. Schinke, J. Koput, S. Stamatiadis, and S. C. Farantos, J. Chem. Phys. **112**, 77 (2000).
[9] M. Joyeux, D. Sugny, M. Lombardi, R. Jost, R. Schinke, S. Skokov, and J. Bowman, J. Chem. Phys. **113**, 9610 (2000).
[10] T. Yamashita and S. Kato, J. Chem. Phys. **119**, 4251 (2003).
[11] R. Hernandez and W. H. Miller, Chem. Phys. Lett. **214**, 129 (1993).
[12] R. Hernandez, J. Chem. Phys. **101**, 9534 (1994).
[13] T. Komatsuzaki and R. S. Berry, J. Chem. Phys. **110**, 9160 (1999).
[14] T. Komatsuzaki and R. S. Berry, Phys. Chem. Chem. Phys. **1**, 1387 (1999).
[15] T. Komatsuzaki and R. S. Berry, J. Mol. Struct.: THEOCHEM **506**, 55 (2000).
[16] T. Komatsuzaki and R. S. Berry, Proc. Natl. Acad. Sci. U.S.A. **98**, 7666 (2001).
[17] T. Komatsuzaki and R. S. Berry, J. Chem. Phys. **115**, 4105 (2001).
[18] T. Komatsuzaki and R. S. Berry, J. Phys. Chem. A **106**, 10945 (2002).
[19] T. Komatsuzaki and R. S. Berry, Adv. Chem. Phys. **123**, 79 (2002).
[20] T. Komatsuzaki and R. S. Berry, Adv. Chem. Phys. **130**, 143 (2005).
[21] T. Uzer, C. Jaffé, J. Palacian, P. Yanguas, and S. Wiggins, Nonlinearity **15**, 957 (2002).
[22] C. Jaffé, S. Kawai, J. Palacián, P. Yanguas, and T. Uzer, Adv. Chem. Phys. **130**, 171 (2005).
[23] S. Kawai, C. Jaffé, and T. Uzer, J. Phys. B **38**, S261 (2005).
[24] C.-B. Li, A. Shojiguchi, M. Toda, and T. Komatsuzaki, Few-Body Syst. **38**, 173 (2006).
[25] C.-B. Li, A. Shojiguchi, M. Toda, and T. Komatsuzaki, Phys. Rev. Lett. **97**, 028302 (2006).
[26] M. Toda, T. Komatsuzaki, T. Konishi, R. Berry, and S. Rice, eds., Adv. Chem. Phys. **130A**, 337 (2005), and references therein.
[27] S. Wiggins, *Normally Hyperbolic Invariant Manifolds in Dynamical Systems* (Springer- Verlag, New York, 1991).
[28] S. Kawai, Y. Fujimura, O. Kajimoto, and T. Yamashita, J. Chem. Phys. **124**, 184315 (2006).
[29] R. D. Levine, *Molecular Reaction Dynamics* (Cambridge University Press, New York, 2005).
[30] A. Deprit, Celest. Mech. **1**, 12 (1969).
[31] A. J. Dragt and J. M. Finn, J. Math. Phys. **20**, 2649 (1979).
[32] V. I. Arnol'd, V. V. Kozlov, and A. I. Neishtadt, *Mathematical Aspects of Classical and Celestial Mechanics* (Springer- Verlag, New York, 1988).
[33] J. Moser, Commun. Pure Appl. Math. **11**, 257 (1958).
[34] H. Akagi, Y. Fujimura, and O. Kajimoto, J. Chem. Phys. **111**, 115 (1999).
[35] W. H. Press, S. A. Teukolsky, W. T. Vetterling, and B. P. Flannery, *Numerical Recipes in C* (Cambridge University Press, Cambridge, 1992).
[36] H. Waalkens, A. Burbanks, and S. Wiggins, J. Chem. Phys. **121**, 6207 (2004).
[37] C.-B. Li, Y. Matsunaga, M. Toda, and T. Komatsuzaki, J. Chem. Phys. **123**, 184301 (2005).
[38] R. B. Shirts and W. P. Reinhardt, J. Chem. Phys. **77**, 5204 (1982).
[39] R. B. Shirts and W. P. Reinhardt, J. Chem. Phys. **79**, 3173 (1983).
[40] A. C. Luntz, J. Chem. Phys. **73**, 5393 (1980).
[41] E. J. Kruus, B. I. Niefer, and J. J. Sloan, J. Chem. Phys. **88**, 985 (1987).
[42] C. R. Park and J. R. Wiesenfeld, Chem. Phys. Lett. **163**, 230 (1989).
[43] C. B. Cleveland and R. Wiesenfeld, J. Chem. Phys. **96**, 248 (1992).
[44] D. G. Sauder, J. C. Stephenson, D. S. King, and M. P. Casassa, J. Chem. Phys. **97**, 952 (1992).
[45] D. G. Sauder and P. J. Dagdigian, J. Chem. Phys. **92**, 2389 (1990).
[46] A. M. L. Irvine, I. W. M. Smith, R. P. Tuckett, and X.-F. Yang, J. Chem. Phys. **93**, 3177 (1990).
[47] A. M. L. Irvine, I. W. M. Smith, and R. P. Tuckett, J. Chem. Phys. **93**, 3187 (1990).